I C A N S - V

MEETING OF THE INTERNATIONAL COLLABORATION ON

ADVANCED NEUTRON SOURCES

June 22-26, 1981

Thermal Neutron Leakage and Time Structure Measured for Various
Target-Moderator-Reflector Configurations for a Spallation Neutron Source

G.S. Bauer*, W.E. Fischer**, F. Gompf[+], M. Küchle[++],
W. Reichardt[+] and H. Spitzer*

* Institut für Festkörperforschung, Kernforschungsanlage Jülich
  D-5170 Jülich, West Germany

** Schweizerisches Institut für Nuklearforschung
   CH-5234 Villigen, Switzerland

[+] Institut für Angewandte Kernphysik I, Kernforschungszentrum Karlsruhe
   D-7500 Karlsruhe, West Germany

[++] Institut für Neutronen- und Reaktorphysik, Kernforschungszentrum Karlsruhe
   D-7500 Karlsruhe, West Germany

Abstract

Measurements were performed at the Swiss Institute of Nuclear Research of
the integrated thermal neutron leakage, the thermal neutron flux distribution
and the time structure of the thermal neutron field for various configurations
of target, moderator and reflector for a spallation neutron source. Among
them were a cylindrical Pb-Bi-target in a D_2O-tank and a slab target with
a hybrid moderator configuration consisting of a D_2O half tank below and a
reflected H_2O moderator above the target. The results are used to predict
performance data for a spallation neutron source with 500 μs long proton pul-
ses. Although there remains some ambiguity due to non-perfect simulation of
the real situation, correction factors derived from independent measurements
could be used. The effect of beam tubes in the D_2O on the thermal neutron
flux was measured directly.

1. Introduction

The present measurements are part of two studies carried out in the Federal Republic of Germany and in Switzerland to assess the feasibility and expected performance of a neutron source for beamhole research, based on the spallation reaction. The design goal of the German source being a thermal neutron leakage out of the beamholes equivalent to that of a reactor with a flux of $6 \cdot 10^{14}$ cm^{-2} sec^{-1}, the heat removal from the target becomes a major problem. To achieve this, two possibilities are considered, namely a flowing-liquid metal /1/ and a rotating solid target /2/. The first concept is also considered for the Swiss project, where a continuous proton beam will be utilized. In the German project a Linac is foreseen which delivers proton pulses of 100 mA peak current and 0.5 msec duration once every 10 msec. In this case the neutron flux will also have a time-structure which is an advantage for many neutron scattering experiments. The degree to which the time structure of the proton beam can be preserved in the neutron flux depends on the type of moderator and reflector chosen. Generally there will be a tradeoff between pulse width and average neutron flux. It was the purpose of the present measurements to provide a basis for the comparison of the various arrangements shown in Fig. 1, namely

- a flat target plate in a D_2O-tank representing a rotating solid target in a large moderator tank (slab target),

  a slab target with the D_2O-tank only half filled and with a polyethylene moderator and reflector above the target representing a hybrid arrangement where one part of the moderator is trimmed for maximum peak flux whereas the other part should provide as high an average flux as possible.

- a cylindrical Pb-Bi-target in a D_2O-tank representing the liquid metal target concept.

In the case of the rotating target both, Pb and U-238 were investigated as possible target materials.

2. Experimental Arrangement

The measurements were performed in the PM1 experimental area of the SIN where a scattered 590 MeV proton beam from the production target E can be used. This beam is deflected and shaped by a series of deflection magnets, variable collimators and focussing elements. It was directed onto a graphite scatterer viewed by a telescope of scintillator counters operated in coincidence to allow quantitative proton beam monitoring. The graphite scatterer was originally placed at a distance of $\sim$ 4 m from the target. The telescope was calibrated by reducing the beam current to a level where direct counting was possible and by comparing the number of coincidences recorded to the number of protons counted in the direct beam. The ratio at the initial setup was

$$G_1 = 312,8 \cdot 10^3 \text{ protons per coincidence recorded.}$$

The profile of the proton beam was monitored by wire-chambers placed in front of (and, for the purpose of alignment, also behind) the target position (Fig. 2). The proton beam profiles obtained in the horizontal and vertical directions
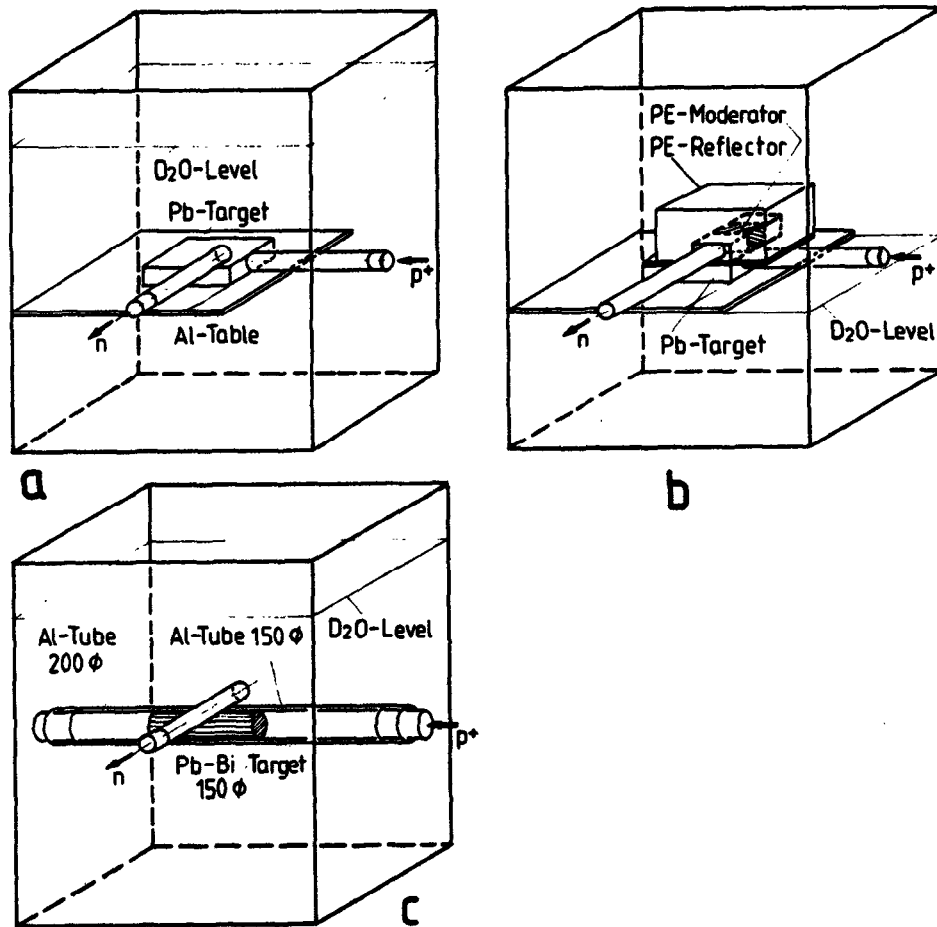
Fig. 1: Schematic representation of target-moderator-reflector arrangements used.

a) Slab target in D_2O-tank
b) Slab target with hybrid moderator configuration (D_2O below target and "H_2O" moderator with reflector above target)
c) Cylindrical target in D_2O-tank

B : BENDING MAGNET
Q : QUADRUPOLS
V : VACUUM TUBE

S : CARBON SCATTERER
MC : MONITOR COUNTERS
     IN COINCIDENCE
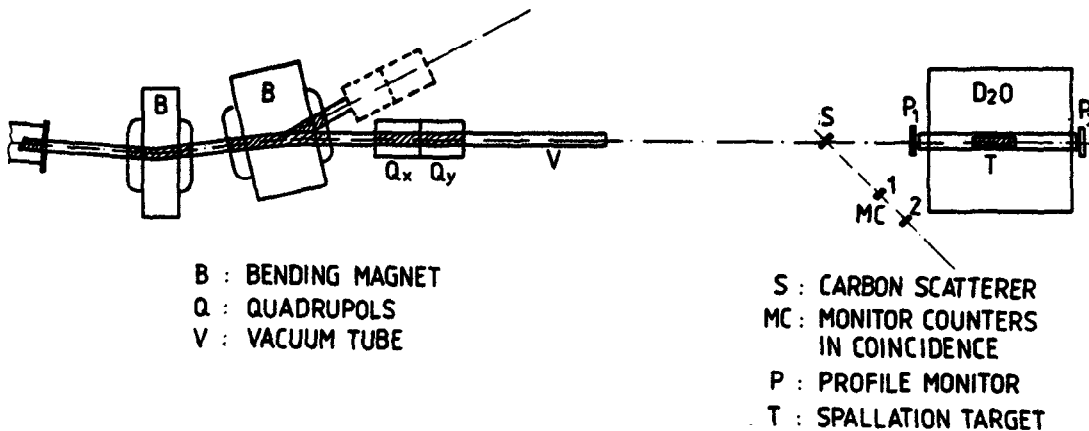P : PROFILE MONITOR
T : SPALLATION TARGET

Fig. 2: End of proton beam line in the PM1 experimental area at SIN as used for the neutron source mock-up studies.

before and after the target are shown in Fig. 3. Although the beam could be properly aligned relative to the target, it was not possible to obtain as narrow a beam profile as desired. During a subsequent attempt to improve the situation (after measurement # 18), it was found that this beam blurring was due to beam scattering in the graphite. With the graphite placed at 2 m from the target, the situation was considerably improved. The calibration factor for the relocated scintillator counter telescope was determined as

$$G_2 = 336.6 \cdot 10^3 \text{ protons per coincidence.}$$

Redoing the same experiment with the now much better focussed beam showed a gain of a factor of F_1 = 1.15 (Measurement # 19 relative to # 18). This gain was initially considered as due in part to protons missing the target in the older arrangement and in part to an increased probability for an internuclear cascade with the better focussed beam. Later on it was found, however, that other measurements yielded almost identical results before and after the change. (# 30 relative to # 12 and # 63 relative to # 8 + # 9). Hence it is concluded, that measurement # 18 must have been slightly in error.

The targets used were placed inside a tank of stainless steel 170 x 170 cm² wide and 250 cm high which could be filled with heavy water up to a level of 170 cm. For the measurements with the cylindrical target (Pb-Bi, 150 mm diameter 600 mm long) the proton beam port was a 150 mm Al-tube coaxially placed inside a 200 mm diameter Al-tube to allow for space needed in a real design (Fig. 4). A total of 10 mm Al was present between the Pb-Bi and the D_2O.

For the simulation of the rotating target, an Al-table of an effective thickness of 30 mm was placed 5 cm below the mid-plane of the tank. The target was built up of Pb bricks or U-238 bricks of 10 cm height and 5 cm thickness interlaced with 6 mm thick polyethylene sheets to simulate the coolant inside the structure (Fig. 5). Similarly, 6 mm of polyethylene were placed above and below the target
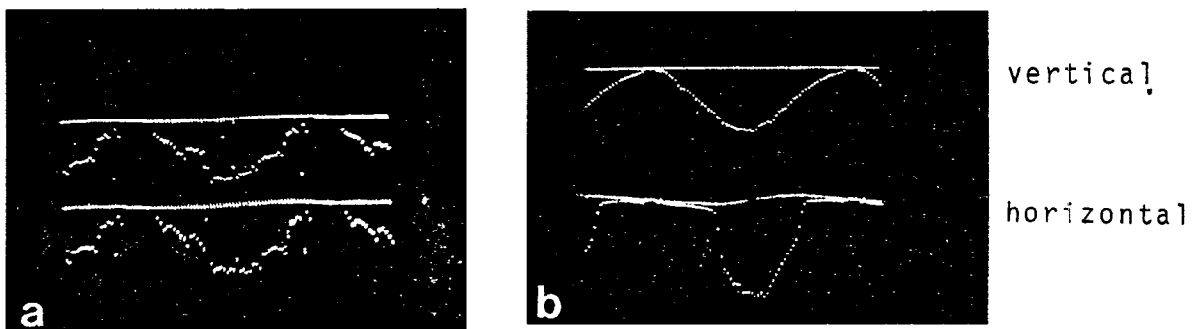

Fig. 3: Proton beam profiles as measured by wire chambers in the initial setup

    a)   in front of target (1 m from head of target). The separation between wires is 1 mm giving a FWHM of about 35 mm for both, the horizontal and the vertical direction.

    b)   behind target (2 m from first chamber). The separation between wires is 2 mm, giving a FWHM of 66 mm in the vertical direction. In the horizontal direction the profile is cut off by the target whose central 5 cm of material had been removed to show correct positioning.
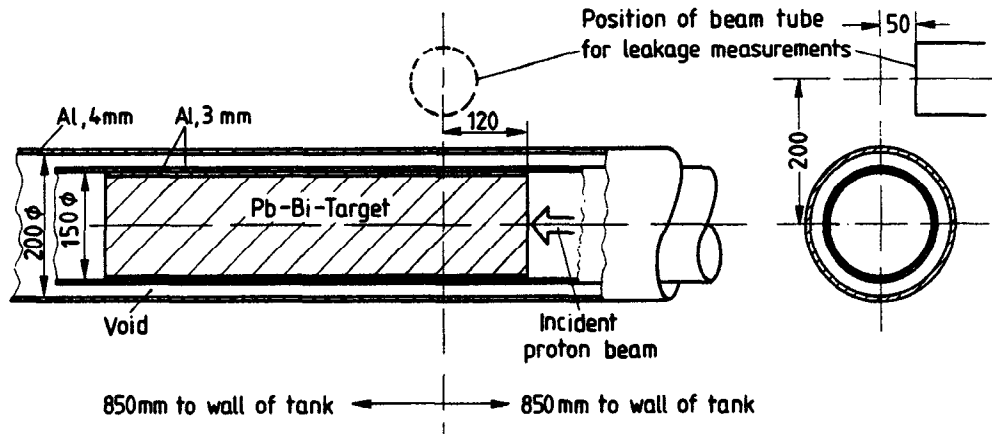
Fig. 4: The cylindrical target used as a mock-up for a liquid Pb-Bi target
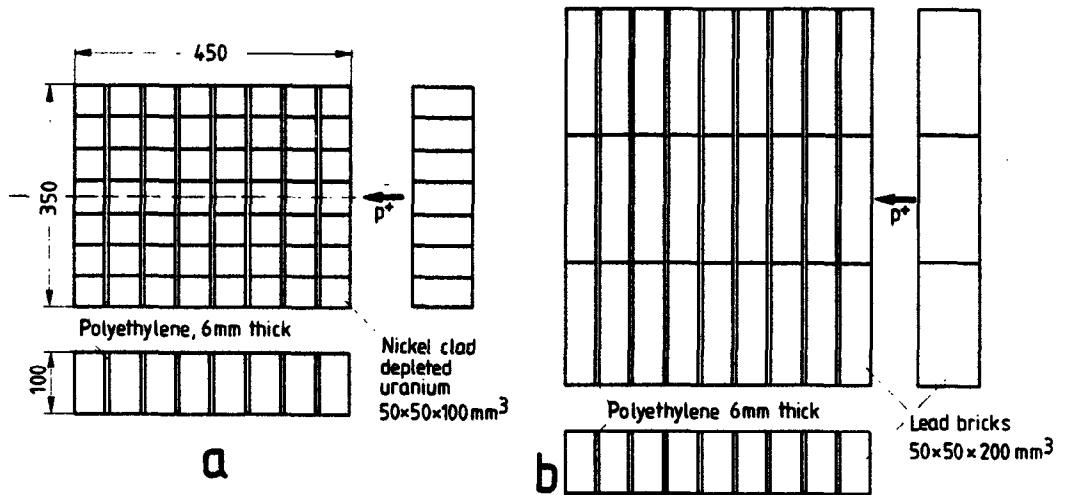system. Dimensions are given in mm.

Fig. 5: The slab targets used as mock-up for the rotating target concept.

a) Depleted uranium target
b) Lead target

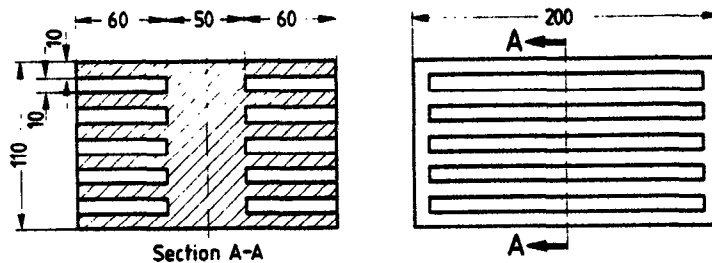The positions of proton incidence are marked by arrows.

Fig. 6: The polyethylene moderator: a 50 mm thick polyethylene slab at the
centre with 60 mm long and 10 mm thick fins on both sides.

with 20 mm of Al on the top. The slab targets were not extended all the way through the tank but only in the central part (35 cm wide for U-238 and 60 cm wide for Pb), but this can be considered as a sufficiently good representation regarding fast neutron yield as well as thermal neutron flux depression. The proton beam was entering through a 100 mm diameter Al-tube. Another 100 mm Al-tube was placed above the target at 12 cm (10 cm for uranium) downstream of the face of proton entry to serve as a thermal neutron beam hole for leakage measurements. For the hybrid moderator version only the lower half of the tank was filled with D_2O. A polyethylene (PE) moderator composed of a massive central part of 50 mm thickness, 120 mm high and 200 mm long and of two parts with 10 mm thick and 60 mm deep fins on either side was placed on top of the target (Fig.6). It was surrounded by a polyethylene reflector 600 mm long, 500 mm wide and 270 mm high. To measure the thermal neutron flux and time distribution, small BF_3-detectors were placed in a thimble below the target in the D_2O and between the fins of the polyethylene moderator.

The following configurations were investigated

A   U-238 slab target in D_2O-tank

B   U-238 slab target with hybrid moderator-reflector configuration

C   U-238 slab target with no D_2O in tank; PE moderator and reflector

D   U-238 slab target with no D_2O in tank; PE moderator, no reflector

E   Pb slab target in D_2O-tank

F   Pb slab target with hybrid moderator-reflector configuration

G   Pb slab target with hybrid moderator configuration; no PE-reflector

H   Pb slab target with no D_2O in tank; PE moderator and reflector

I   Pb slab target with no D_2O; PE moderator, no reflector

K   cylindrical target; tank filled with D_2O

L   Pb slab target in D_2O-tank with PE moderator immersed in D_2O

Pos.	r (cm)
(3)	4.2
(4)	10
(5)	20
(6)	24

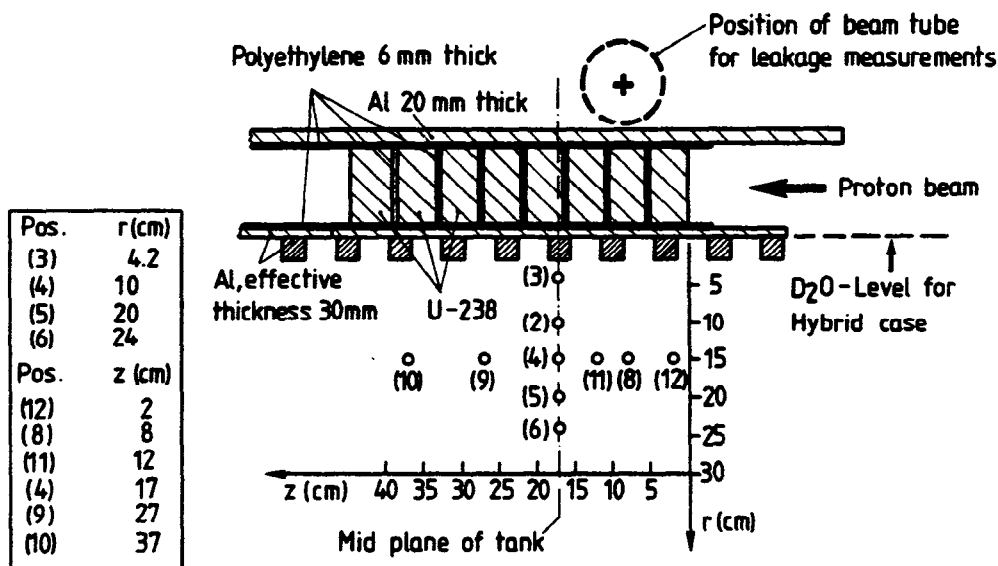| Pos.	z (cm)
(12)	2
(8)	8
(11)	12
(4)	17
(9)	27
(10)	37

Fig. 7: Positions in the D_2O below the target, where flux measurements with the BF_3-detector were taken.

The individual measurements have been labelled by consecutive numbers which are underlined in this report. Some of them being runs for testing and checking purposes, not all will be reported here.

3. Thermal neutron flux distribution

Although a more detailed investigation of the thermal neutron flux distribution using Dy-foil activation has been carried out /3/, we did a crude survey of the flux distribution in the D_2O by moving the small BF_3-detector to different positions in order to be able to assess the flux at the position of our leakage measurement relative to the maximum flux and to compare by direct counting the flux in the full D_2O-tank to that in the semi-tank of the hybrid version. The
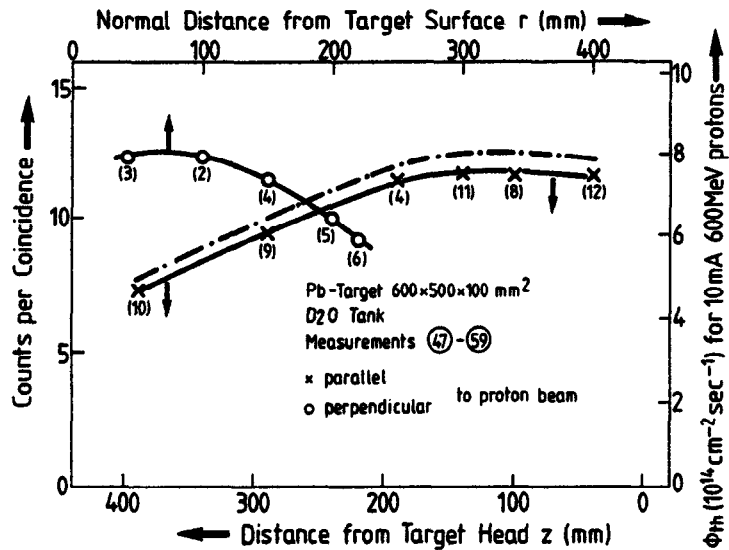
Fig. 8. Thermal neutron flux distribution measured for the case of a slab target of lead in a D_2O-tank. The dash-dotted curve gives the values corrected for the radial position of maximum flux.
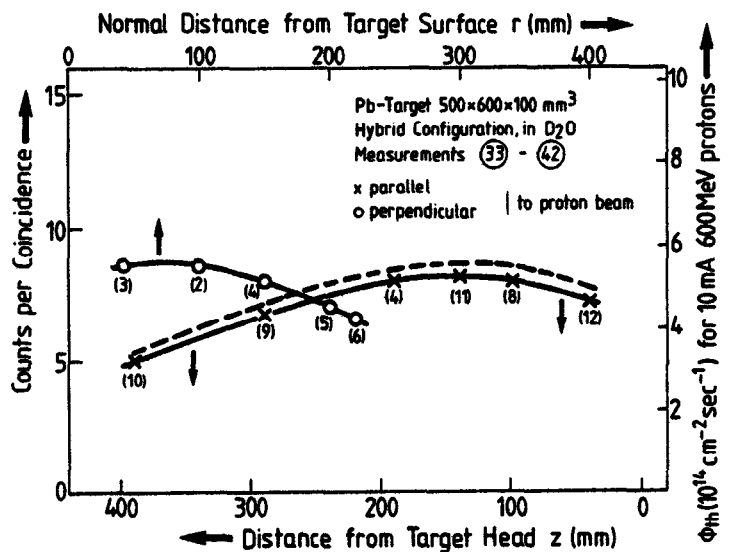
Fig. 9: Thermal neutron flux distribution measured for the case of a slab target of lead in the D_2O part of a hybrid moderator configuration. The dashed curve gives the axial distribution corrected for the maximum radial flux value.

positions, where flux measurements were taken for the slab target are shown in
Fig. 7. The flux distributions measured in the directions parallel and perpendi-
cular to the proton beam are shown in Figs. 8 through 11. There was only a limi-
ted region of accessibility with the Al-thimble holding the detector. The flux
values given at the right hand scales have been derived from the neutron leakage
measurements as described below.

For the case of the lead target the measurements parallel to the proton beam
were not in the maximum flux region. A curve corrected by the ratio of the inten-
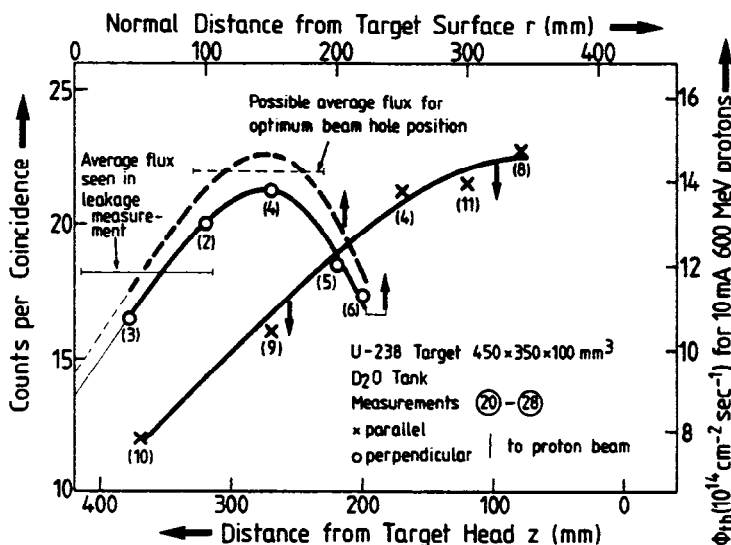sities at the respective maxima of the parallel and perpendicular distributions

Fig. 10: Thermal neutron flux distribution measured for the case of a slab
target of depleted uranium in a D_2O-tank. The dashed curve gives the
normal distribution as corrected for the maximum value along the
target. The horizontal lines give the range actually averaged over
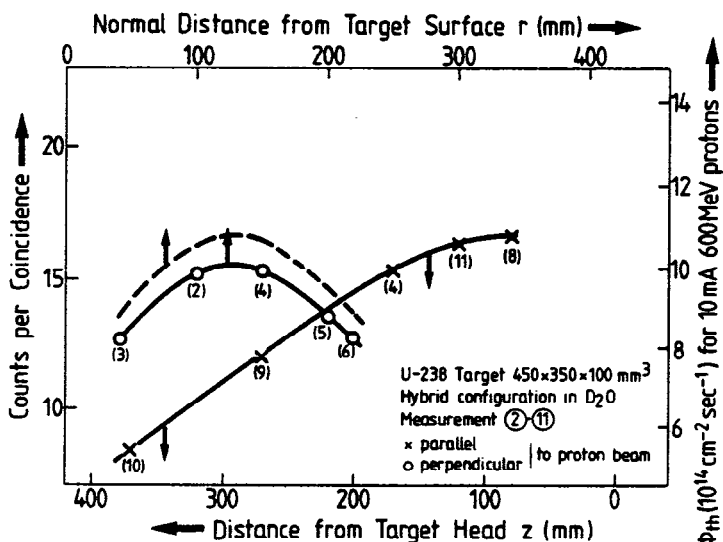by the beam tube (solid) and the possible best position (dashed).

Fig. 11: Thermal neutron flux distribution measured for the case of a slab
target of depleted uranium in the D_2O part of a hybrid moderator
configuration. The dashed curve gives the normal flux distribution
corrected for the maximum value along the target.

is given by the broken lines in Figs. 8 and 9. For the lead target the thermal neutron flux in the D_2O of the hybrid arrangement is by a factor of $F_2 = 0.72$ lower than in the full tank. Here the measured hybrid configuration has to be considered as a worst case limit because in a real arrangement some neutron back scattering would occur from the then present lead shield above the D_2O-tank.

In the case of the uranium target the flux distribution perpendicular to the proton beam was not taken at the position of the maximum of the parallel distribution. Therefore a dashed curve scaled with the ratio of the maximum fluxes measured in both directions is also given in the plots. Since the measurements in the U-target hybrid version (Fig. 11) were done before the repositioning of the carbon scatterer mentioned above, there is some uncertainty about the magnitude of the flux relative to the subsequent measurements. However no correction was attempted according to what was said in the previous chapter. Similar to the case of the lead target, the flux in the hybrid version is down by a factor of 0.74 relative to the full tank. Some, but relatively less improvement may also be expected in this case, if a complete target and lead shielding is present in the real situation. Also marked in Fig. 10 is the distance from the target surface which was viewed by the beam hole for the leakage measurements. Obviously, in order to obtain maximum leakage, the position should have been as indicated by the dashed horizontal line. The gain that would have been obtained is the ratio of the average fluxes at these positions which is

$$F_3 = 1.2 .$$

This factor will be used for the comparison of maximum leakage. (This factor depends slightly on the extrapolation used towards the target surface but the possible uncertainty is small.)

From Fig. 8 to 11 it is obvious that the uranium target causes a severe flux depression in the surrounding D_2O with the peak flux shifted some 15 cm away from the target surface, whereas in the case of lead the flux stays high up to the target surface. This has some effect on the optimum distance of the beam holes from the target surface, in particular since the fast neutron and γ-flux will decrease much more rapidly with distance than the thermal neutron flux.

Table 1 gives a listing of corrected count rates for the peak fluxes and the peak flux positions. Also included is the ratio of the flux 25 cm further downstream from the target head to the peak flux (measuring position (8)). This

Target	Configuration	Peak Flux			$\dfrac{I_{25}}{I_{max}}$
		z(mm)	r(mm)	I_{max}	
Pb	D_2O-Tank	120	70	12.6	0.65
Pb	Hybrid	140	70	8.8	0.60
U-238	D_2O-Tank	80	150	22.5	0.61
U-238	Hybrid	80	130	16.7	0.59
Pb-Bi	Cylinder in D_2O-Tank	120	75	13.8	0.80

Table 1: Comparison of thermal neutron count rates for various target moderator configurations. For I_{max} the corrected peak values have been taken (in units of counts per proton coincidence). I_{25} is the value 25 cm downstream from the position of maximum flux at the same radial distance.

ratio is only slightly lower for the uranium target. The more concentrated source of primary neutrons in the uranium is largely smeared out by the D_2O. More detailed investigations of the thermal neutron flux distributions in the moderators will be reported separately. The flux distribution for the cylindrical target had been measured earlier /3/. The result is shown in Fig. 12. No direct comparison of the flux level to the present measurement is possible but from the thermal neutron leakage results reported in the following chapter, a relative value for I_{max} can be deduced which is $I_{max} = 13.9$. This has been included in Table 1.
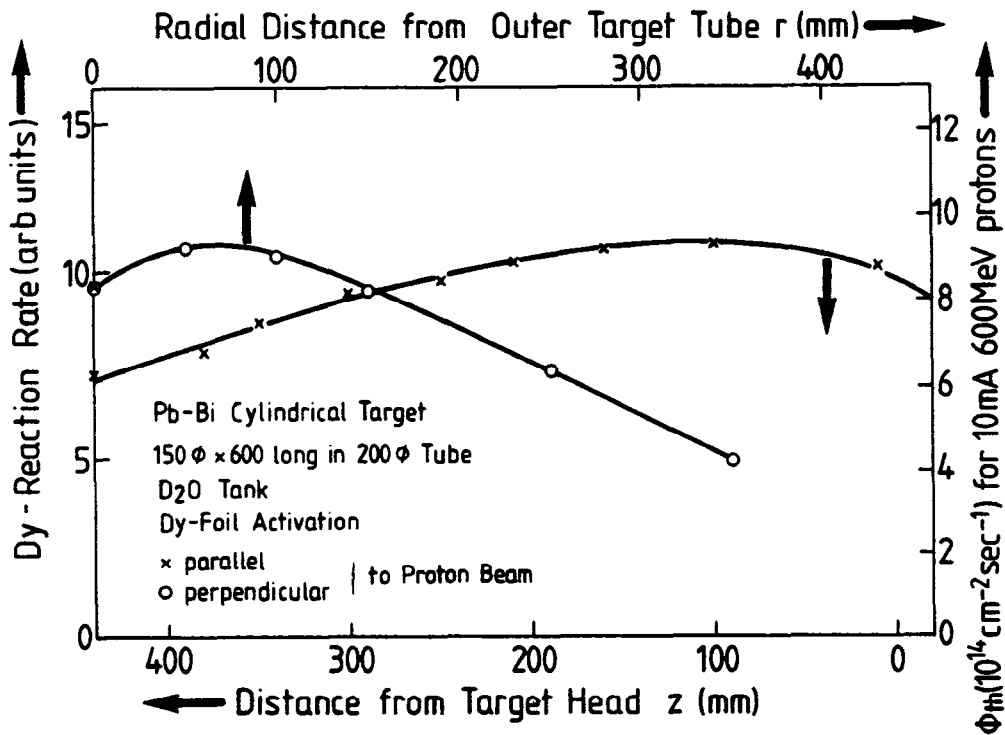

Fig. 12: Thermal neutron flux distribution in a D_2O-tank surrounding a Pb-Bi target of 150 mm $\emptyset$ and 600 mm length placed concentrically in a 200 mm diameter Al-tube (Fig. 4) as measured by Dy-foil activation. The figure shows the Dy-reaction rate as a function of position.

4. Thermal neutron leakage from the moderators

4.1 Comparison of target-moderator-reflector configurations

In order to be able to compare the thermal neutron leakage from the various moderators, measurements were made on an extracted neutron beam with a fixed

geometry for all moderators. The setup is shown in Fig. 13. The detector used
was a BF_3-proportional counter with 23 mm diameter and an average detection
efficiency over the cross section of

$$\varepsilon = 0.056$$

for a thermal neutron spectrum. The active height was limited to 50 mm by a
Cd slit and the effective solid angle was determined by a Cd diaphragm of
50 mm diameter placed at 2330 mm from the detector. The detector was looking
at the bottom of a 100 mm diameter beam tube inserted in the D_2O-tank, which,
for all measurements using the flat targets, ended at 10 cm from the central
plane of the tank. For the measurements using the cylindrical target, the beam
hole ended at a radius of 20.5 cm from the centre line of the target.

Data were taken for a preset number of coincidences of the proton monitor with
and without a 2 mm cadmium sheet inserted at the position marked(A) in Fig. 13.
The difference of the two recordings gives the thermal neutron counts, Z_0.
A list of results is given in Table 2.

From these data it can be seen that the D_2O in the hybrid configuration has some
effect on the leakage from the PE-moderator (12 % gain for the U-target and 30 %
gain for the Pb-target). It is therefore of interest to look whether the D_2O is
merely acting as a fast neutron reflector or whether there is a noticeable
effect on the thermal neutron time structure. We will come back to this in
chapter 5.

The efficiency of the polyethylene moderator is also different for the various
configurations. With no D_2O present it is smaller than with D_2O present under
the target. This indicates that D_2O acts more as a reflector for fast neutrons
than for thermal ones, since the mean freee path of thermal neutrons in poly-
ethylene is small. Also the lower efficiency in the case of the U-238 target
relative to the Pb-target can be qualitatively understood, because for the
U-target the primary source of fast neutrons is more concentrated under the
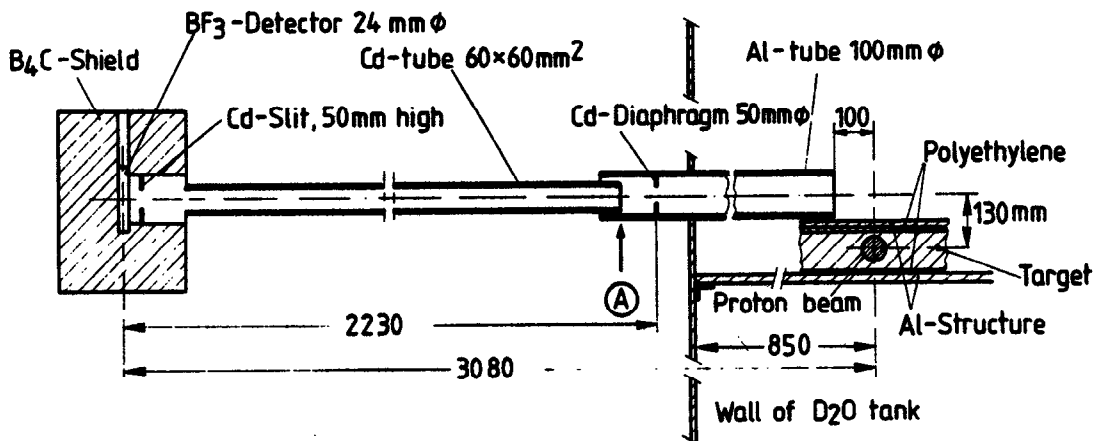moderator itself.

Fig. 13: Schematic representation of the setup used for the thermal neutron
leakage measurements.

Measurement	Configuration	Target	upper moderator	upper reflector	lower moderator + reflector	Z_0 (2 x 10^5 coinc.)	G 10^3 p/coinc.	Z_0^* (10^{-7} n/p)
(18	A	U-slab	D_2O	D_2O	D_2O	10925	312.8	1.75)
19		"	"	"	"	13770	336.6	2.05
64		"	"	"	"	13217	336.6	1.96
8 + 9	B	U-slab	PE	PE	D_2O	8572	312.8	1.37
63		"	PE	PE	"	8857	336.6	1.32
12 + 16	C	U-slab	PE	PE	-	7465	312.8	1.19
17	D	U-slab	PE	-	-	5673	312.8	0.91
30		"	PE	-	-	6132	336.6	0.91
46	E	Pb-slab	D_2O	D_2O	D_2O	8700	336.6	1.29
66		"	"	"	"	8818	336.6	1.31
32	F	Pb-slab	PE	PE	D_2O	4295	336.6	0.64
65		"	PE	PE	"	4340	336.6	0.65
62	G	Pb-slab	PE	-	D_2O	2494	336.6	0.37
31	H	Pb-slab	PE	PE	-	3359	336.6	0.50
60	I	Pb-slab	PE	-	-	2375	336.6	0.35
61		"	PE	-	-	2410	336.6	0.36
72 + 7	K	Pb-Bi cyl.	D_2O	D_2O	D_2O	9661	336.6	1.44 1.58
57	L	Pb-slab	PE	D_2O	D_2O	8365	336.6	1.24

Table 2: Thermal neutron counts per proton for the various target-moderator-reflector configurations investigated. All leakage measurements were taken at the upper moderator. ([+]Measurement 7 was done in an earlier period, see footnote on page 11)

The Z^*-values, which give the number of thermal neutrons recorded per 600 MeV-proton incident on the target, are not directly relevant for the expected performance the neutron source because the actual configuration has not been simulated properly in these experiments. Corrections to be applied will be discussed in chapter 6.

For the D_2O-moderators, some flux depression will occur due to further beam holes placed in the moderator. This effect has also been investigated and will be reported in the following section.

4.2   Effect of additional beam holes in the D_2O

4.2.1 Cylindrical Pb-Bi target[1]

The effect of beam holes in the D_2O on the thermal neutron leakage from a given tube has been investigated by inserting 10 empty Al tubes of 10 cm diameter in the tank, in addition to the one used for the measurement. The extra tubes were arranged in two planes with 5 tubes in each plane and placed at distances of 15 cm upstream and downstream of the reference tube. They were suspended on a mechanism which allowed to change the positions of the noses of the 5 tubes in one plane simultaneously relative to the target centre line. The noses were placed at r = 20 and r = 40 cm. The results obtained without the extra tubes and with the tubes in place are given in Table 3. It can be seen that the overall flux depression by having as many as 11 beam tubes in the tank is relatively small (18 % for r = 20 cm). It should be noted, that one of the extra tubes was very close to the standard tube. A radial position of 20 cm corresponds to r' = 100 cm in Fig. 12. The axial positions of the tubes would be z = 250 and z =   - 50 mm. It can be seen that the flux at these positions is still very close to the maximum value.

Measurement	Number of tubes in place	Radial position of extra tubes	$Z_0^*(10^{-7}n/p)$
1	1	–	1.58
2	11	20 cm	1.26
3	11	40 cm	1.34

Table 3: Effect of additional beam holes in the D_2O-tank for a Pb-Bi cylindrical target

4.2.2 Pb-slab target

In order to estimate the effect of additional beam holes placed in the D_2O in the case of a slab target, a set of runs was performed, where beam holes were consecutively removed from the D_2O, starting with a configuration as shown in Fig. 14. In the region above the target there were effectively 6 beam tubes with four of them arranged as two twin tubes. This means that the two tubes shared

---

[1] These measurements were done in a different measuring period where the calibration yielded an absolute neutron to proton ratio which is 10 % higher than obtained in the period where most of the measurements were done. The numbers for the beam tube effect have not been corrected for this fact.
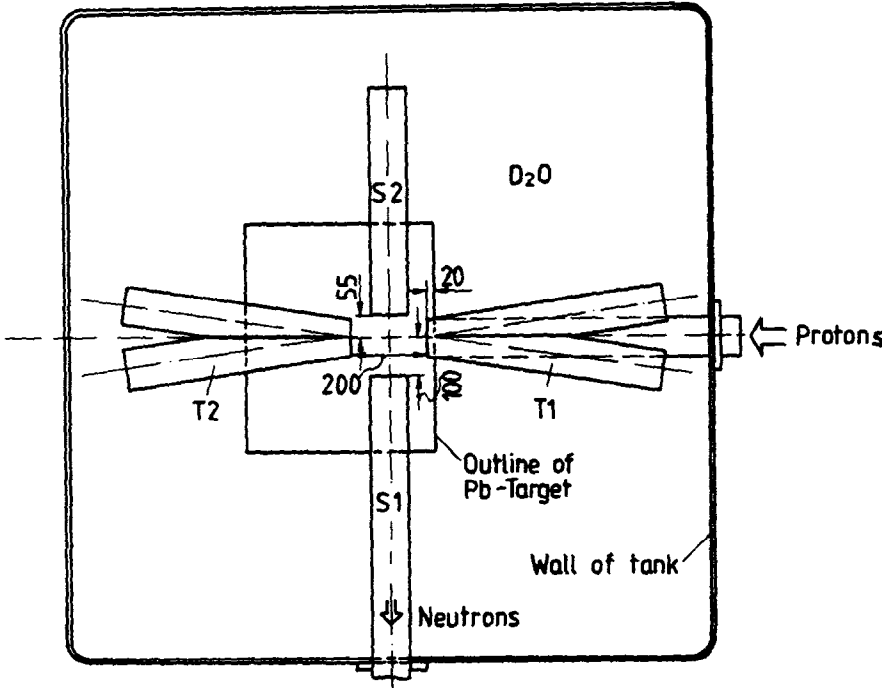
Fig. 14:

Arrangement of beam-tubes used for the measurement of the resulting flux depression for the case of a lead slab target. Beam tubes are in the plane above the target. T1 and T2 are twin tubes and S1 and S2 are standard tubes of 10 cm diameter. The neutrons leaking out of S1 were measured.

one common bottom from which two tubes of 100 mm diameter emerged with an angular separation of 15°. In this way the amount of D_2O displaced can be reduced relative to two single beam tubes. Two of the tubes (including the one on which the measurements were made) were single beam tubes. Table 4 lists the measured leakage values with different numbers of tubes in place. The tubes T1 und T2 had slightly different positions relative to S1 but in general it can be said, that the effect of both, twin tubes and single tubes is small with an overall flux depression of 13 % occuring in response to five additional holes in the same half of the moderator. From the little crosstalk observed before, it can be expected that beam holes in the lower half of the tank would hardly affect the upper half at all.

Measurement	Tubes in place	$Z_0^*(10^{-7} n/p)$	ΔZ^*
67 / 68	S1, S2, T1, T2	1.12	
69	S1, S2, T2	1.19	0.07
70	S1, S2	1.25	0.06
71 / 46	S1	1.29	0.04
			0.17

Table 4: Measured neutron leakage for the Pb-slab target in D_2O with different beam tubes in place.

5. Time structure of the neutron field in the moderators

Since it is foreseen in the German project that the proton beam shall hit the target in pulses of 0.5 ms duration once every 10 ms, it is of interest to predict the time structure of the resultant thermal neutron field in the different concepts considered. To this end measurements were made with the secondary beam of the cyclotron pulsed by means of a mechanical chopper placed near the entrance of the PM1 beam line. The chopper consisted of a spinning hollow Al-cylinder of 1 cm wall thickness and 9 cm outer diameter with 2 slits of 1 cm width at its circumference. When the 2 cm of Al were in the beam, its energy was sufficiently degraded that the following bending magnet system did not transport it through the downstream collimator. The idea was that intensity should be transmitted only, when the two slits allowed the proton beam to pass through unperturbed. The chopper was spun at 100 rps which resulted in a proton pulse every 5 ms. The time structure of the proton intensity hitting the target is shown in Figs. 15a and 15b. The pulse of Fig. 15a was obtained with the original setup, the one of Fig. 15b after the realignment mentioned above which took place after measurement number 18. In both cases, the pulse is well des-
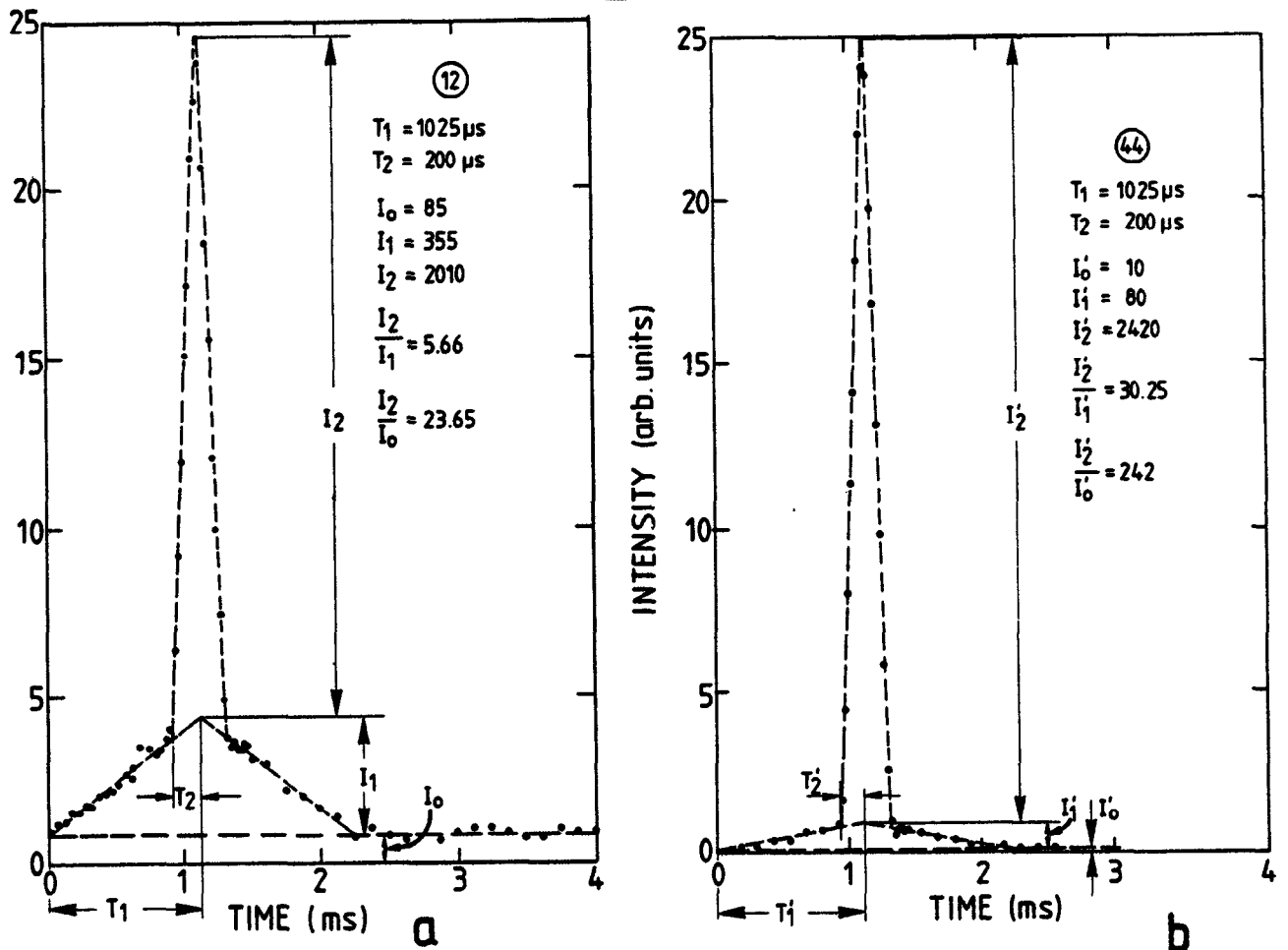

Fig. 15: Time structure of proton pulses as measured by the scintillator telescope for the chopped PM1-beam.

a) Graphite scatterer at 4 m from target (i.e. before realignment of beam.

b) Graphite scatterer at 2 m from target (i.e. after realignment of beam).

cribed by two triangles superimposed upon one another plus a constant background. The base widths of the triangles were very near to constant. Only a slight variation was observed for the various measurements, as can be seen from Table 5. The ratio between the intensities of background and the two triangles, also contained in Table 5, showed somewhat stronger variations. With such a proton pulse, the resulting time structure of the neutron pulse is easily predictable, if the time needed for thermalisation is neglected and a decay constant α is assumed.

Measurement	T_1 (μs)	T_2 (μs)	$\dfrac{I_2}{I_o}$	$\dfrac{I_2}{I_1}$	$\dfrac{I_2^*}{I_o}$	$\dfrac{I_2^*}{I_1}$	F
1	1125	200	22.6	6.58	94.9	9.9	0.908
12	1125	200	23.6	5.66	99.1	8.5	0.895
29	1000	200	173	22.8	-	-	0.956
44	925	200	160	30.2	-	-	0.966
45	1050	187.5	235	36.1	-	-	0.973
74	1050	200	165.5	37.8	-	-	0.974

Table 5: Characteristics of the proton beam time distributions as determined in the various measurements. The values marked by an asterix are obtained by correcting I_o and I_1 by factors of 4.2 and 1.5 respectively, as described in the text.
F is given by $F = (1-I_1/I_2)^{-1}$.

With the notation given in Fig. 15 and using E as a coupling constant which relates the neutron flux to the proton beam intensity[1] we obtain for

$$0 \le t \le T_1 - T_2 \qquad \Phi' = \Phi_0 + \Phi_1^1$$

$$T_1 - T_2 \le t \le T_1 \qquad \Phi' = \Phi_0 + \Phi_1^1 + \Phi_1^2$$

$$T_1 \le t \le T_1 \pm T_2 \qquad \Phi' = \Phi_0 + \Phi_2^1 + \Phi_2^2$$

$$T_1 + T_2 \le t \le 2T_1 \qquad \Phi' = \Phi_0 + \Phi_2^1 + \Phi_3^2$$

$$2T_1 \le t \qquad \Phi' = \Phi_0 + \Phi_3^1 + \Phi_3^2$$

---

[1] E is, of course, a function of geometry and the materials used and is considered, for the time being, as an adjustable parameter.

with

$$\Phi_0 = E \cdot I_0 \cdot \lim_{t \to \infty} \int_0^t e^{-\alpha(t-t')} dt = \frac{E \cdot I_0}{\alpha}$$

$$\Phi_1^1(t) = E \cdot \frac{I_1}{T_1} \cdot \frac{1}{\alpha^2} \left\{ e^{-\alpha \cdot t} + \alpha \cdot t - 1 \right\}$$

$$\Phi_2^1(t) = E \cdot \frac{I_1}{T_1} \cdot \frac{1}{\alpha^2} \left\{ e^{-\alpha(t-T_1)} (e^{-\alpha T_1} - 2) - \alpha(t-2T_1) + 1 \right\}$$

$$\Phi_3^1(t) = E \cdot \frac{I_1}{T_1} \cdot \frac{1}{\alpha^2} \left\{ e^{-\alpha(t-T_1)} 2[\cosh(\alpha \cdot T_1) - 1] \right\}$$

$$\Phi_1^2(t) = E \cdot \frac{I_2}{T_2} \cdot \frac{1}{\alpha^2} \left\{ e^{-\alpha(t-T_1+T_2)} + \alpha(t-T_1+T_2) - 1 \right\}$$

$$\Phi_2^2(t) = E \cdot \frac{I_2}{T_2} \cdot \frac{1}{\alpha^2} \left\{ e^{-\alpha(t-T_1)} (e^{-\alpha T_2} - 2) - \alpha(t-T_1-T_2) + 1 \right\}$$

$$\Phi_3^2(t) = E \cdot \frac{I_2}{T_2} \cdot \frac{1}{\alpha^2} \left\{ e^{-\alpha(t-T_1)} 2[\cosh(\alpha \cdot T_2) - 1] \right\} \tag{1a}$$

Frame overlap of z pulses due to a separation T_3 between proton pulses can be taken into account by putting

$$\Phi(t,\alpha) = \Phi_0(\alpha) + \sum_{n=1}^{n=3} \sum_{m=1}^{m=2} \sum_{l=0}^{z-1} \Phi_n^m \left((t + 1 \cdot T_3), \alpha \right) \tag{1}$$

5.1 The polyethylene moderator

It is likely that, in a small hydrogeneous moderator, one decay constant α is sufficient to describe the time dependence of the neutron field. This view is supported by the slope of the trailing edge of the neutron pulses measured for the polyethylene moderator as shown in Fig. 16 b and 17 b. The decay constants derived from these slopes are not the true decay constants due to the contribution of the proton pulse to the pulse width. An approximate correction can be obtained by using the second moment as time resolution. With the resolution function given by a sum of two triangles with base widths $2T_1$ and $2T_2$ and fractional heights (1-F) and F, the second moment is

$$\int_{-\infty}^{\infty} t^2 R(t) dt = \frac{(1-F) \cdot T_1^3 + F \cdot T_2^3}{6[(1-F) \cdot T_1 + F \cdot T_2]} = \sigma^2 \tag{2}$$
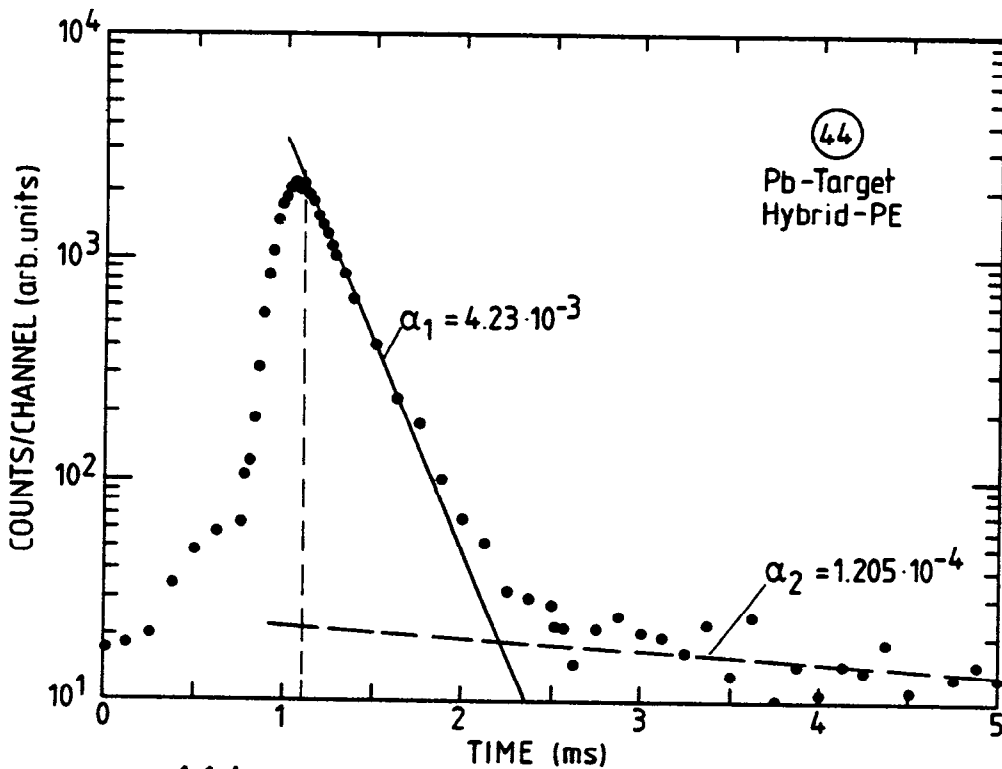
16a

16 b
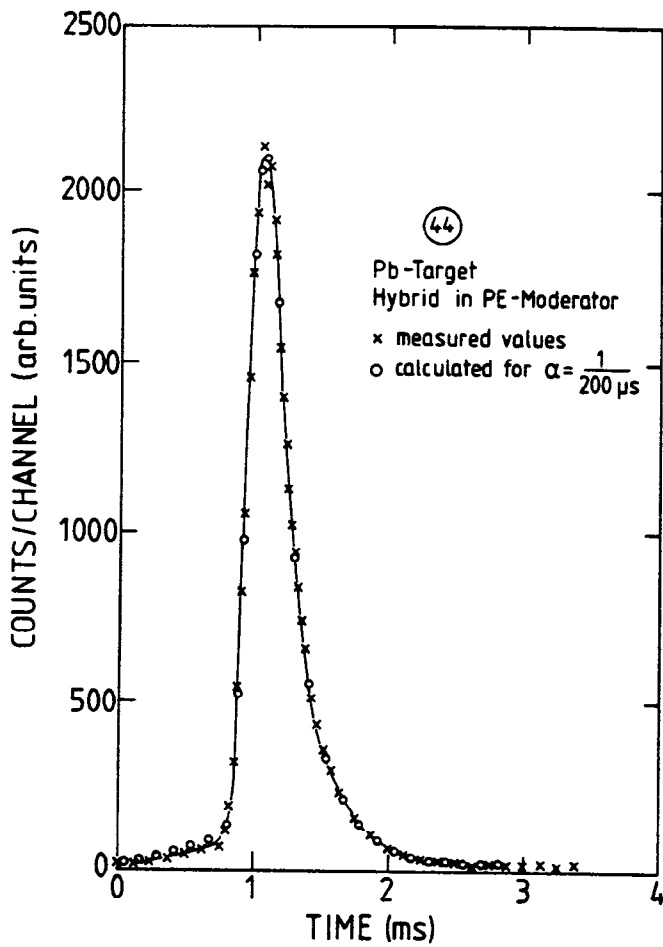
Fig. 16:

Time structure of the neutron field
in the polyethylene moderator of
the hybrid configuration with a
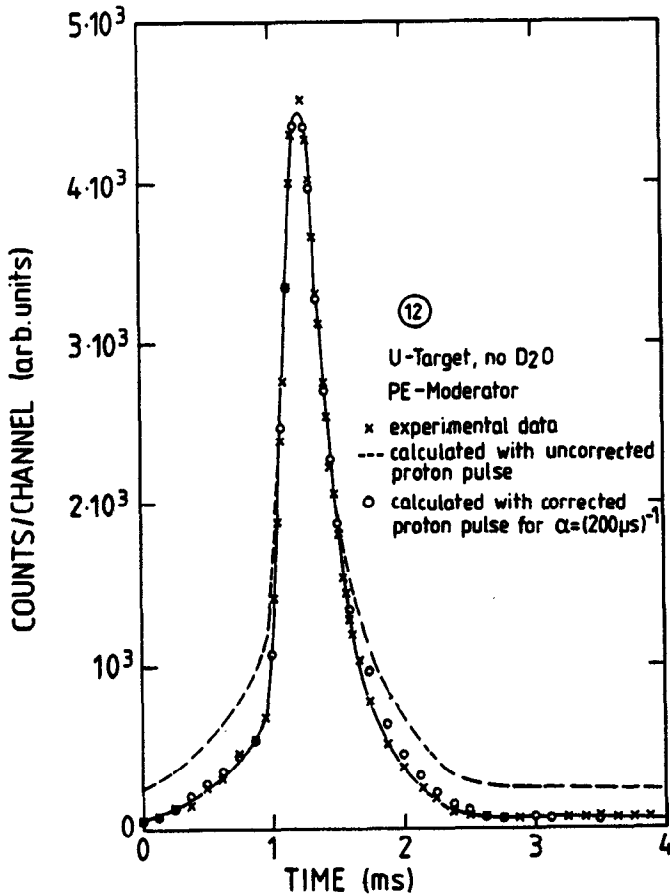Pb-target. (measurement $\underline{44}$)

a) linear plot, solid curve is a
   guide to the eye through the
   measured data (crosses) open
   circles are values calculated
   with equ. (1) and

   $\alpha = \dfrac{1}{200 \ \mu s}$ and the proton
   pulse of Fig. 15b.

b) logarithmic plot showing that
   decay is dominated by one
   single life time.

Fig. 17:

Time structure of the neutron field in the polyethylene moderator with a target of depleted uranium and no D_2O present in tank (measurement # 12)

a) linear plot, solid curve is a guide to the eye through the measured data (crosses).

The dashed curve was obtained, using equ. (1) and $\alpha = (180 \ \mu s)^{-1}$ with the proton pulse as shown in fig. 15a.

Open circles are values calculated with equ. (1) and $\alpha = (200 \ \mu s)^{-1}$ and with the proton pulse corrected as described in the text.

b) Logarithmic plot showing one decay constant.

17a
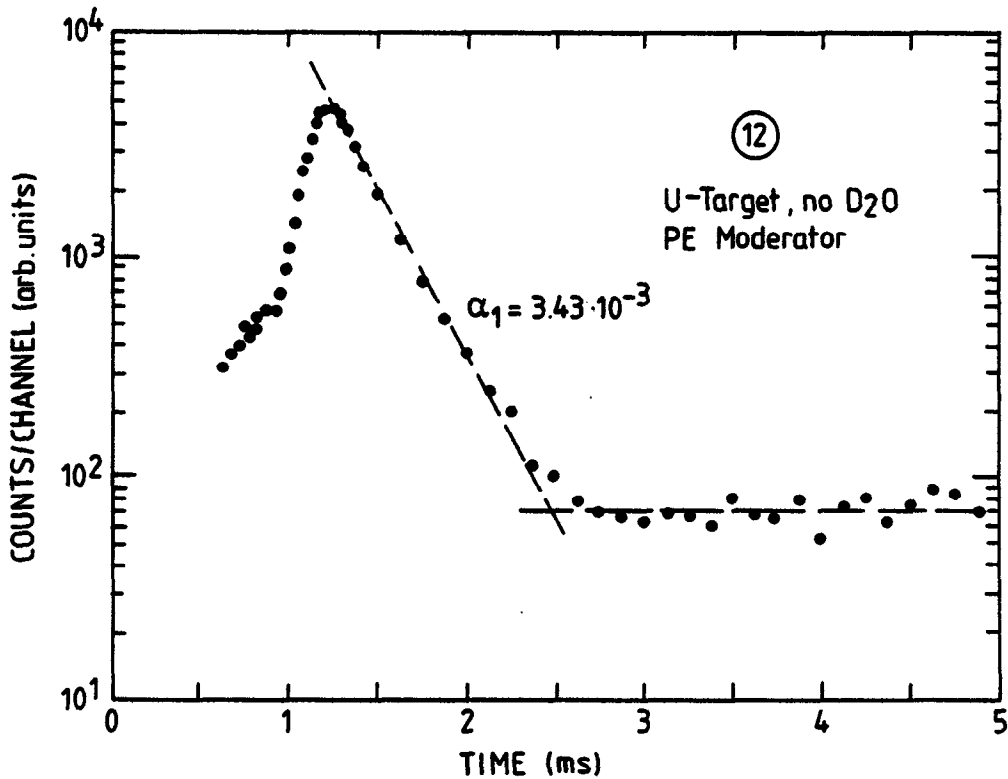
17b

For the proton distribution of Fig. 15b, using the values of Table 5, this yields

$$\sigma_p = 160.3 \ \mu s$$

Since the second moment of an exponential decay is given by $\sigma_{exp}^2 = 2\tau^2$, we obtain for the "true" decay time

$$\tau^* = \sqrt{\tau^2 - \frac{\sigma_p^2}{2}}$$

(3)

which leads to $\tau^* = 207 \ \mu s$ for the case of Fig. 16.

In Fig. 16a the open circles represent a calculation with equ. (1) and a decay time of 200 μs using the proton pulse of Fig. 15b. The result can be seen to agree reasonably well with the measured data. Attempting a similar fit for the case of a curve measured with the proton pulse shown in Fig. 15a yielded curve b (dashed) in Fig. 17a, which has been adjusted to the measured data at the peak value. Obviously the calculated background is much higher than the measured one and also the rise in the part where $t < T_1 - T_2$ is significantly faster than measured. This indicates that not all of the background proton current and of the proton intensity in the wide triangle seen by the monitor at 4 m from the target actually hit the target. This can be qualitatively understood by the way the chopper worked, since it is assumed that the background in caused by insufficient energy degradation when the proton beam was blocked by one wall of the hollow chopper only. If the background contribution and the intensity in the wider triangle are scaled down by factors of 4.2 and 1.5 respectively, the values given in Fig. 17a by open circles are obtained from equ. (1) with $\alpha = (200 \ \mu s)^{-1}$.

In Fig. 18, the curves measured for the case of a slab target of depleted uranium with and without D_2O present under the target are shown, normalized to the same number of measured proton coincidences. There is a 10 % increase in peak intensity due to the D_2O but practically no long time effect on the intensity. This shows that the D_2O acts mainly as a reflector for fast neutrons and that the uranium target is a sufficiently good decoupler for thermal neutrons to prevent any significant cross talk.

This is even true to a large extent for a lead target as can be seen from Fig. 16. Only a very small tail with a long decay constant is noticeable in Fig. 16b, corresponding to less than 1 % of the peak intensity.

Due to the different shapes of the proton pulses in the various measurements, the peak intensities obtained for a fixed number of proton coincidences are not directly comparable among one another. Under the condition that the total number of protons remain constant for the pulses characterized by primed and unprimed quantities one has:

$$I_1 \cdot T_1 + I_2 \cdot T_2 = I_1' \cdot T_1' + I_2' \cdot T_2'$$

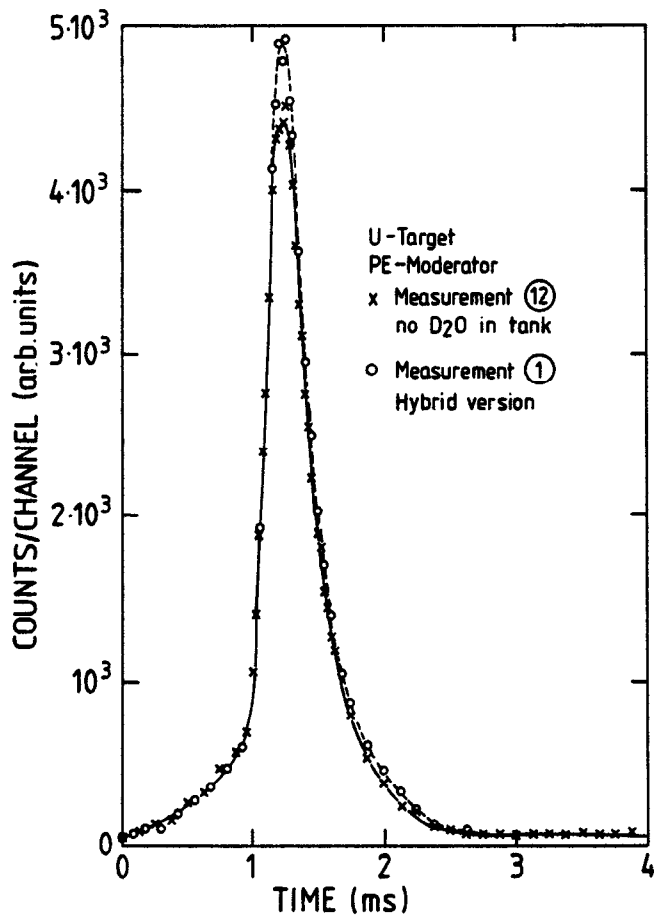In our case we have $T_1 \approx T_1'$ and $T_2' \approx T_2'$.

Fig. 18:

a) Comparison of neutron time
   distributions measured for
   equal numbers of protons
   for a polyethylene modera-
   tor and a unranium target
   without (solid curve) and
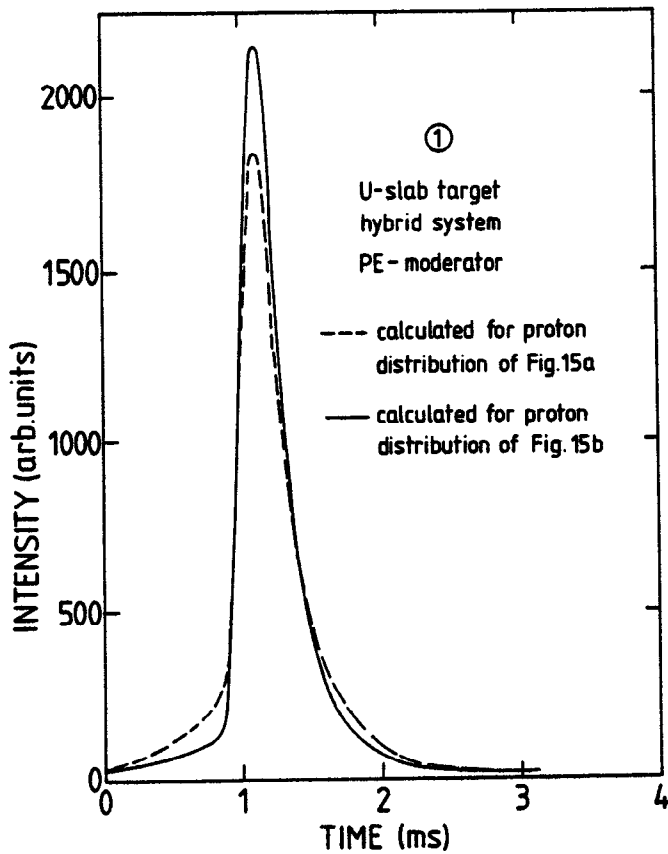   with D_2O under the target
   (dashed curve).

Fig. 19:

Computed curve of neutron time
distribution for the polyethylene
moderator of the hybrid configu-
ration with a proton distribu-
tion as shown in Figs. 15a and
15b.

This yields

$$I_1' = \frac{I_1 + I_2 \dfrac{T_2}{T_1}}{1 + \dfrac{I_2'}{I_1'} \cdot \dfrac{T_2}{T_1}} \tag{4}$$

where the ratio I_2'/I_1' is known.

Inserting numbers for measurements $\underline{1}$ and $\underline{44}$ (primed) from Table 5 we have

$I_1^* = 80$ p/channel, $\quad I_2 = 790$ p/channel, $\quad I_2'/I_1' = 30.2$,

$T_1 = 1025$ µs, $\quad T_2 = 200$ µs which leads to

$I_1' = 34$ p/channel, $\quad I_2' = 1025$ p/channel.

I_o is not affected.

The actual correction factor depends also on the decay constant α and can be determined relatively easily if one time constant is clearly dominating as for the case of the polyethylene moderator. The curve that would have been obtained in the case of the U-target for a proton distribution as in Fig. 15b can thus be computed for comparison to the Pb-target. It is shown in Fig. 19.

The resulting increase in peak intensity is by a factor of 1.18. A direct comparison between peak intensities on a per proton basis is difficult from the time structure measurements because the various measurement were done in different positions. However, the leakage measurements can be used to get ratios of mean intensities which can be converted to peak intensities if the shape of the proton pulse is known. An example will be given later.

5.2 The D_2O moderator

For the case of the heavy water tank the analysis of the measured time distributions is less simple due to the fact that

- more than one time constant is contributing to the decay behaviour
- frame overlap is important in the measured data.

Although a more sophisticated analysis is in progress, the following simple approach, that was used for the time being, is believed to give reasonably accurate results already:

It was assumed that only two time constants α_1 and α_2 are important with the respective fractions $D \cdot E \cdot I$ and $(1-D) \cdot E \cdot I$ decaying in these modes. Hence

$$\Phi(t, \alpha_1, \alpha_2) = D \cdot \Phi(t, \alpha_1) + (1-D) \cdot \Phi(t, \alpha_2) \tag{5}$$

with $\Phi(t, \alpha_1)$ calculated according to equ. (1). The effect of the background between proton pulses was negelcted[1]. In order to obtain a first set of input

---

[1] For large contributions from slowly decaying modes this is probaly the major source of error.

parameters for a calculation, the measured data were plotted on a semiloga-
rithmic plot and straight line was drawn through the long-time part of the
curve. These values were subtracted from the measured data to yield another
straight line whose slope was taken as the measured value of the fast decay
constant α_1. This was corrected for resolution according to equ. (3) to yield
α_1^*. Frame overlap was taken into account in a global manner by drawing a
third straight line parallel to the first one such that its value for T = 0
was the same as that of the first one for T = 5 ms. This line was used as a
base-line to read the slope of the first one (α_2) and the relative intensites
of the fractions decaying with the two time constants. This latter reading was
taken near the position of the apparent maximum of the curve. The procedure
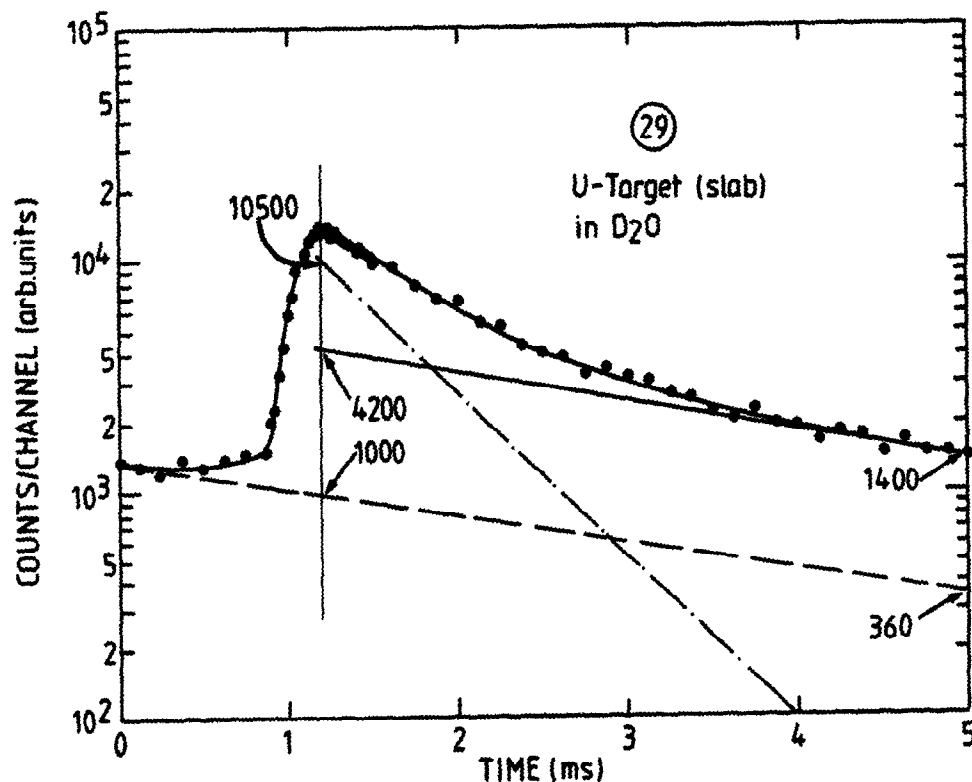is examplified in Fig. 20 for measurement 29.

Fig. 20: Semilogarithmic plot of the thermal neutron time structure measured
for a U-238 slab target in a D_2O tank. The solid straight line has
been adjusted to the slope of the data at large t. The difference
between the measured data (curve through data) and the solid line
is given by the dash-dotted line. The dashed line represents the
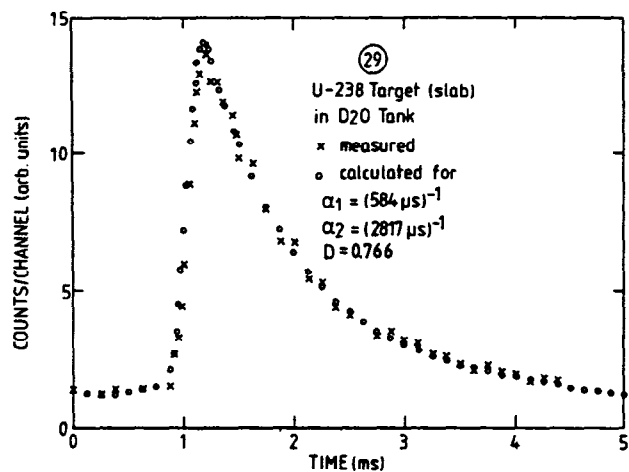frame overlap from previous pulses.

For this case we have

$$\alpha_1 = \frac{\ln 1050 - \ln 100}{2800 \; \mu s} = 1.66 \cdot 10^{-3} \; \mu s^{-1}$$
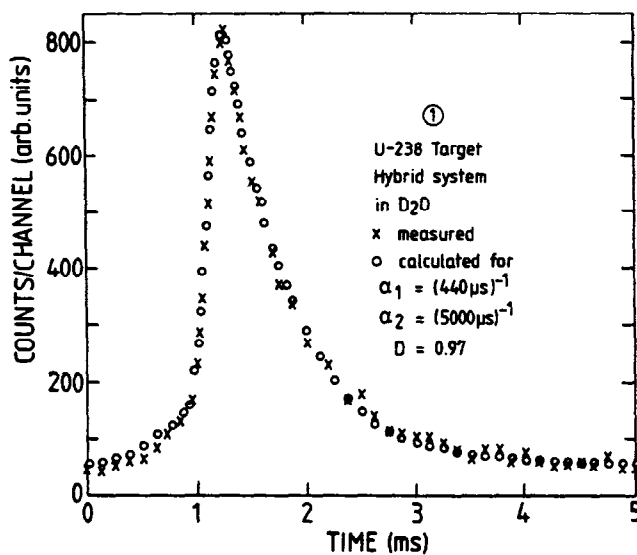
$$\alpha_2 = \frac{\ln (4200 - 1000) - \ln (1400 - 360)}{(5000 - 1200 \; \mu s)} = 0.296 \cdot 10^{-3} \; \mu s^{-1}$$

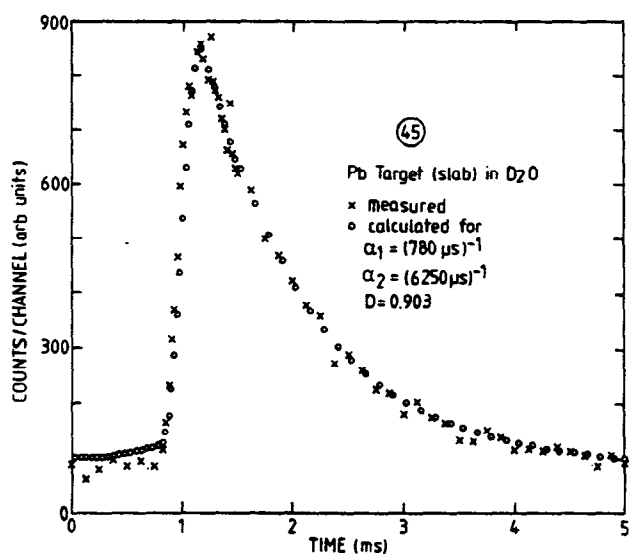$$\frac{\Phi_o(\alpha_1)}{\Phi_o(\alpha_2)} = \frac{10500}{4200 - 1000} = 2.97 = \frac{D \cdot \Phi_o}{(1-D) \cdot \Phi_o}$$

or D = 0.766
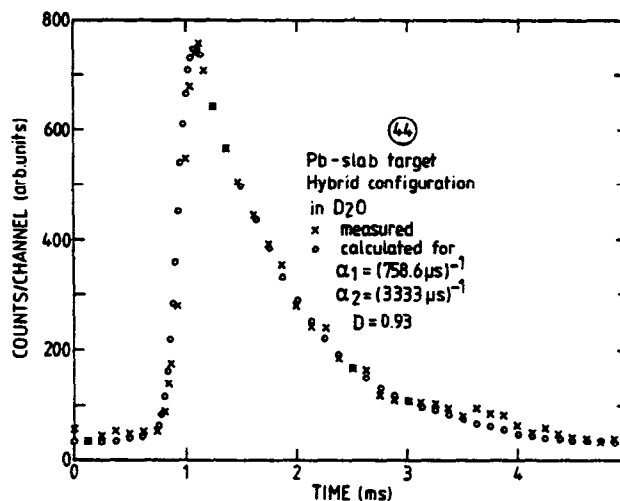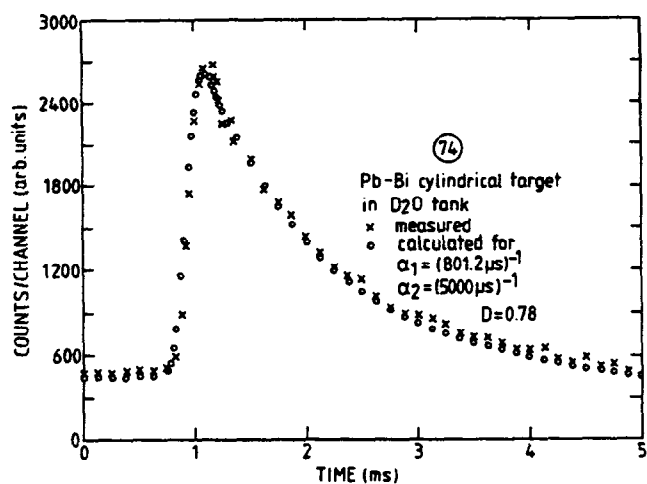
Fig. 21:

Measured time structure in the D_2O for various target-moderator configurations.

a) U-238 slab target in D_2O
b) U-238 slab target with hybrid moderators
c) Pb-slab target in D_2O
d) Pb-slab target with hybrid moderators
e) Pb-Bi cylindrical target in D_2O

Crosses give measured data, circles are the result of calculations with the parameters indicated.

Measurement	Configuration		α_1 $10^{-3} \mu s^{-1}$	τ_1 (µs)	α_2 $10^{-3} \mu s^{-1}$	τ_2 (µs)	D	σ (µs)	τ_1^* (µs)	α_1^* $10^{-3} \mu s^{-1}$	τ_2^* (µs)	α_2^* $10^{-3} \mu s^{-1}$	D*
1	U–Hyb	PE	3.384	295.5	–	–	1	296.44	208.4	4.80	–	–	1
		D₂O	1.89	529.6	0.230	4348	0.890	296.44	440.0	2.27	5000	0.200	0.97
12	U	PE	3.43	291.0	–	–	1	308.0	193.0	5.18	–	–	1
29	U	D₂O	1.66	600.0	0.296	3381	0.766	191.3	584.5	1.71	2817	0.355	0.766
44	Pb–Hyb	PE	4.227	226.3	0.121	8290	0.996	160.3	195.9	5.1	8290	0.121	1
		D₂O	1.304	767	0.300	3330	0.80	160.3	758.6	1.32	3333	0.300	0.930
45	Pb	D₂O	1.286	790	0.137	7300	0.903	172.6	780.5	1.28	6250	0.160	0.903
74	Pb–Bi	D₂O	1.233	810	0.195	5128	0.670	168.6	801.2	1.25	5000	0.200	0.780

Table 6: Decay parameters for the various target-moderator configurations. The unmarked values have been derived from semilogarithmic plots of the measured data. Values marked by an asterix are those used to calculate the values given by circles in Fig. 21.

The values thus obtained are summarized in Table 6. Using these values to cal-
culate the curves according to equ. (5) did not result in a satisfatory agree-
ment with measured data. Therefore α_2 and, if necessary also D was varied to
improve the agreement. In this way the values α_2^* and D^* given in Table 2 were
obtained[1]. Figs. 21a through 21e show the curves calculated with these data
and the (corrected) proton pulse parameters of Table 5. In view of the assump-
tions made (see above) it did not seem reasonable to try and further improve
the fits. The decay parameters thus obtained are considered sufficient to
estimate the time structure expected for a different shape of the proton pulse.

6. Discussion

6.1 Thermal neutron flux

As mentioned in chapter 4.1, the Z^*-values obtained in the present measurements
are not in all cases representative for the expected performance of a real
spallation source because:

- in the case of the uranium slab target the flux at the measuring position
  was by a factor of 1.2 down from the flux at the "best" position,

- the polyethylene reflector used in these measurements is much less efficient
  than the combination of Be-reflector and Pb-shield foreseen for the projec-
  ted German source. From earlier experiments /4/ it is known that a factor
  of 3 can be gained relative to an unreflected moderator. The gain by the
  polyethylene reflector used here was roughly 1.4. The fact, that PE rather
  than H_2O was used as a moderator in these measurements does not affect the
  thermal neutron leakage in a reflected geometry as has been shown earlier
  /4/.

A set of "best" Z_0^{**}-values obtained by taking these corrections into account,
is given in Table 7 for the various target-moderator-reflector combinations.
The values given for the D_2O moderators in the hybrid systems have been dedu-
ced from the full tank values using the ratio of measured thermal neutron
fluxes. They have to be considered as lower limit values because the albedo
of the air above the D_2O is much less than that of the aluminium and lead which
will be present in a real design. From the effect the D_2O has on the PE-modera-
tor a gain of roughly a factor of 1,3 seems to be likely.

It is of interest to note that, despite the fact that a considerable flux de-
pression occurs near the uranium target, the thermal neutron leakage from the
D_2O moderator is almost twice that for a Pb-target (ratio 1.85 in good agree-
ment with the value of 1.8 obtained in the flux measurements).

Also given in Table 7 is a figure which represents the isotropic thermal neu-
tron flux in D_2O delivering the same neutron current as a spallation source
operated at 600 MeV, 10 mA (roughly equivalent to 1100 MeV, 5 mA) with the
given configuration. This value is obtained from the geometry of the setup
used for the measurement and the efficiency of the detector, ϵ. Allowing for
the fact that the current at a moderator surface, j, is given by /5/.

$$j = \frac{\Phi}{2}$$

---

[1] For the case of the D_2O in the U-target hybrid version it was necessary to
vary also α_1 and take a constant background into account.

Configuration	Moderator	Correction factor	Z_0** $(10^{-7}$ n/p)	$\overline{\Phi}_{equ}$ $(10^{14}$cm^{-2}sec$^{-1})$	$\dfrac{\hat{\Phi}}{\overline{\overline{\Phi}}}$
U-238 rotating target in D_2O tank	D_2O	1.2	2.54	14.7	
U-238 rotating target hybrid version	D_2O	(1.3)	1.9	11.0 (14.4)	10.5
	H_2O	3	2.7	16.7	18.2
Pb-rotating target in D_2O tank	D_2O	1	1.3	8.0	
Pb-rotating target hybrid version	D_2O	(1.3)	0.9	5.6 (7.2)	7.9
	H_2O	3	1.1	6.8	18.4
Pb-Bi flowing liquid target in D_2O	D_2O	1	1.5	9.3	4.6

Table 7: List of "best" neutron leakage values and corresponding equivalent thermal neutron flux (at 600 MeV, 10 mA) for the various configurations considered. Values of $\overline{\Phi}_{equ}$ in parenthesis are guesses taking into account the albedo of the materials present in a real design.

one obtains:

$$\overline{\Phi}_{equ} = \frac{8\pi \cdot R^2}{F_1 \cdot F_2} \cdot \frac{Z_0**}{\epsilon}(\frac{n}{p^+}) \cdot I(mA) \cdot 6.25 \cdot 10^{15}(\frac{p^+}{mAs})$$

with $F_1 = 2.3 \cdot 5$ cm^2, $F_2 = 2.5^2\pi$ cm^2, $R = 223$ cm, $\epsilon = 0.056$ and $I = 10$ mA
this yields

$$\overline{\Phi}_{equ} = 6.18 \cdot 10^{21} \cdot Z_0** \text{ cm}^{-2} \text{ sec}^{-1}.$$

The same value of ϵ has been used throughout, because the spectrum in a well reflected H_2O-moderator with grooves should be very similar to that in a D_2O-tank.

6.2 Expected time structure for a rectangular proton pulse

For a rectangular proton pulse of duration t_p and intensity I the time-dependent thermal flux is

$$\phi(t) = \sum_i \Phi_i^{as} \cdot (1-e^{-\alpha_i t}) \qquad \text{for } t < t_p$$

$$\text{and} \quad \phi(t) = \sum_i \Phi_i^{as} \cdot (1-e^{-\alpha_i t_p})(e^{-\alpha_i(t-t_p)}) \quad \text{for } t \geq t_p \qquad (6)$$

where Φ_i^{as} is the contribution of the fraction of neutrons decaying with time constant α_i to the asymptotic value of the flux that would be reached at long times if the proton pulse were on continuously (equ. 1a). For two contributions with time constants α_1 and α_2 and weights D and (1-D) respectively the total asymptotic flux is

$$\Phi^{as} = \Phi_1^{as} + \Phi_2^{as} = \frac{D \cdot E \cdot I}{\alpha_1} + \frac{(1-D) \cdot E \cdot I}{\alpha_2} ,$$

(7a)

or, conversely

$$E \cdot I = \frac{\Phi_{as}}{\dfrac{D}{\alpha_1} + \dfrac{1-D}{\alpha_2}}$$

(7b)

Φ_i^{as} is related to the average flux Φ_i^{av} in a pulsed mode with duty cycle $\Delta = (t_p \cdot \nu)^{-1}$ (ν = repetition rate)

$$\Phi_i^{av} = \Phi_i^{as} \cdot t_p \cdot \nu.$$

(8)

Representative values for Φ^{av} can be obtained from the data of Table 7, if allowance is being made for effects like flux depression due to beamholes and further structural materials where necessary (which will of course also affect the α's). Examples of the expected time dependent flux are shown for the measured cases 44 (PE-moderator of hybrid configuration with Pb slab target) and 74 (Pb-Bi cylindrical target in D_2O with one beam hole present) in Fig. 22.

For the peak-to-average ratio one finds

$$\frac{\hat{\Phi}}{\bar{\Phi}} = \frac{1}{t_p \cdot \nu} \frac{\dfrac{D}{\alpha_1}(1-e^{-\alpha_1 t_p}) + \dfrac{1-D}{\alpha_2}(1-e^{-\alpha_2 t_p})}{\dfrac{D}{\alpha_1} + \dfrac{1-D}{\alpha_2}}$$

(9)

For the two above cases this yields with the data of Table 6:

$$\frac{\hat{\Phi}}{\bar{\Phi}} = 18.4 \text{ for the PE-moderator in the hybrid version}$$

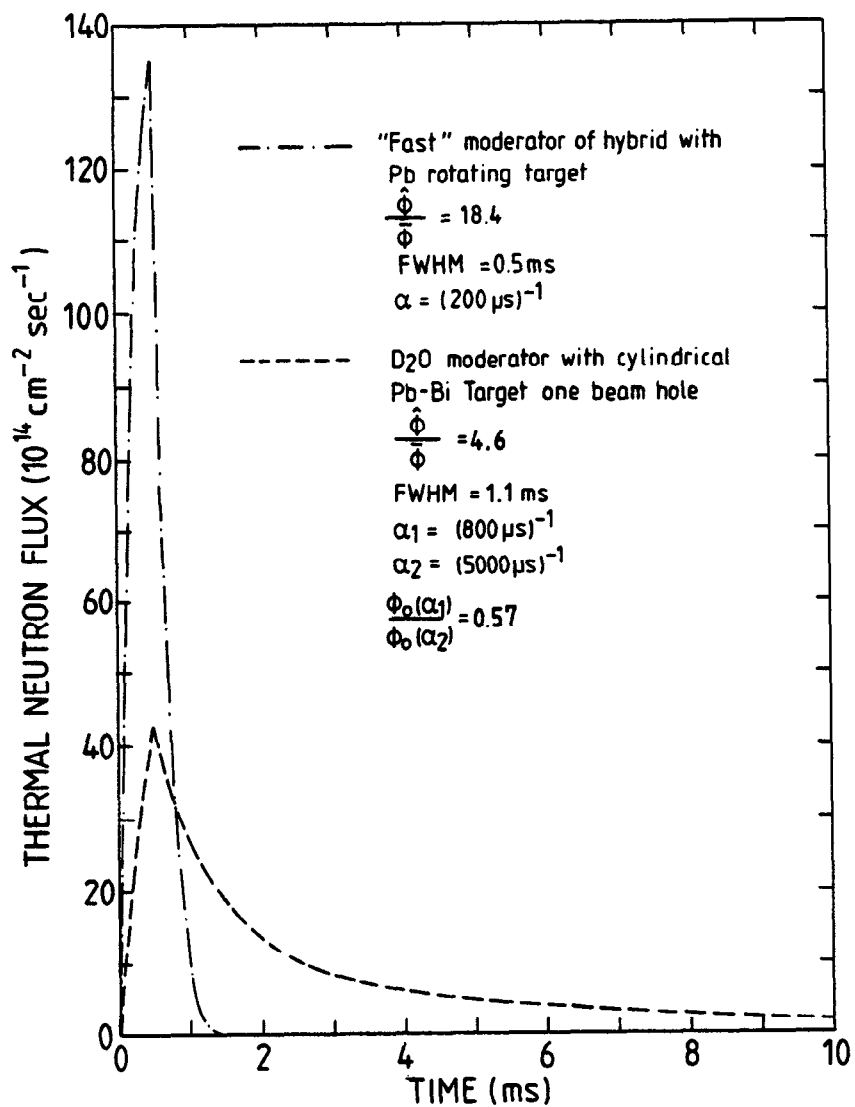$$\frac{\hat{\Phi}}{\bar{\Phi}} = 4.6 \text{ for the Pb-Bi target in the } D_2O\text{-tank}$$

Fig. 22:

Expected time structure of thermal neutron fluxes for the case of a rotating Pb-target with a fast moderaotr (curve a) and a cylindrical Pb-Bi target in a D_2O tank for a 0.5 ms proton pulse of 1100 MeV once every 10 ms.

References

/1/ Hoffmann H., "Prospects for a Liquid Metal Target System for a Spalla-
     tion Neutron Source", (1979), Jül-Conf. 35 pp 127-153

/2/ Bauer G.S., "Design Studies for a Rotating Target Arrangement for a
     Spallation Neutron Source" (1979), Jül-Conf. 35 pp 155-183

/3/ Drüke V., Paul N., Bauer G.S. and Spitzer H., "Measurement of thermal
     neutron flux distributions for various target-moderator configurations
     for a spallation neutron source by activation of Dy-foils", this volume

/4/ Bauer G.S., Gompf F., Mannhardt W., Reichardt W., Scherm R. and
     Spitzer H., "Thermal Neutron Leakage from Hydrogeneous Moderators
     for a Spallation Neutron Source" (1981), SNQ-report, part III A2,
     unpublished

/5/ Beckurtz K.H. and Wirtz K., "Neutron Physics", Springer, Berlin (1964)